Resonance properties of thick plasmonic split ring resonators for sensing applications

Valentina Giorgis,[1,*] Pierfrancesco Zilio,[2] Gianluca Ruffato,[2] Michele Massari,[3] Gabriele Zacco,[1,3] and Filippo Romanato[1,2]

[1]*Istituto Officina dei Materiali, IOM-CNR, S.S. 14 km 163,5 in Area Science Park, 34149 Basovizza, Trieste, Italy*
[2]*University of Padova, Department of Physics and Astronomy, Via Marzolo 8, 35131, Padova, Italy*
[3]*Laboratory for Nanofabrication of Nanodevices, LaNN – Veneto Nanotech, CorsoStatiUniti 4, 35127 Padova, Italy*
**giorgis@iom.cnr.it*

Abstract: We investigate in detail the optical response of dense split ring resonator (SRR) arrays as a function of their thickness, for normally impinging light in the VIS-NIR spectral range. We find that, for sufficiently tall SRRs, several vertical Fabry-Perot resonances can be excited, which may interact with the well-known horizontal SRR resonant paths. Furthermore, we analyze the possibility to exploit these nanostructures to detect bio-chemical quantities. In particular, we find that the coexistence of vertical and horizontal resonances yields an increased sensitivity. Well ordered, large arrays of thick SRRs are obtained by exploiting a fabrication process based on X-Ray Lithography. A very good agreement is found between numerical and measured transmittances. A preliminary detection test evidences the potential of this geometry as a sensing platform.

OCIS codes: (160.3918) Metamaterials; (250.5403) Plasmonics; (260.5740) Resonance; (220.4241) Nanostructure fabrication; (220.3740) Lithography; (280.4788) Optical sensing and sensors; (260.0260) Physical optics.

References and links

1. S. Ramakrishna and T. Grzegorczyk, *Physics and Applications of Negative Refractive Index Materials* (CRC Press, 2009).
2. T. J. Cui, D. R. Smith, and R. Liu, eds., *Metamaterials Theory, Design and Applications* (Springer, 2010).
3. V. M. Shalaev, "Optical negative-index metamaterials," Nat. Photon. **1**(1), 41–48 (2007).
4. S. Linden, C. Enkrich, M. Wegener, J. Zhou, T. Koschny, and C. M. Soukoulis, "Magnetic response of metamaterials at 100 terahertz," Science **306**(5700), 1351–1353 (2004).
5. N. Liu and H. Giessen, "Coupling effects in optical metamaterials," Angew. Chem. Int. Ed. Engl. **49**(51), 9838–9852 (2010).
6. D. R. Smith, W. J. Padilla, D. C. Vier, S. C. Nemat-Nasser, and S. Schultz, "Composite medium with simultaneously negative permeability and permittivity," Phys. Rev. Lett. **84**(18), 4184–4187 (2000).
7. I. M. Pryce, Y. A. Kelaita, K. Aydin, and H. A. Atwater, "Compliant metamaterials for resonantly enhanced infrared absorption spectroscopy and refractive index sensing," ACS Nano **5**(10), 8167–8174 (2011).
8. E. Cubukcu, S. Zhang, Y. S. Park, G. Bartal, and X. Zhang, "Split ring resonator sensors for infrared detection of single molecular monolayers," Appl. Phys. Lett. **95**(4), 043113 (2009).
9. B. Päivänranta, H. Merbold, R. Giannini, L. Büchi, S. Gorelick, C. David, J. F. Löffler, T. Feurer, and Y. Ekinci, "High aspect ratio plasmonic nanostructures for sensing applications," ACS Nano **5**(8), 6374–6382 (2011).
10. A. W. Clark, A. Glidle, D. R. S. Cumming, and J. M. Cooper, "Plasmonic split-ring resonators as dichroic nanophotonic DNA biosensors," J. Am. Chem. Soc. **131**(48), 17615–17619 (2009).
11. J. Naqui, M. Durán-Sindreu, and F. Martín, "Novel sensors based on the symmetry properties of split ring resonators (SRRs)," Sensors **11**(12), 7545–7553 (2011).
12. J. F. O'Hara, R. Singh, I. Brener, E. Smirnova, J. Han, A. J. Taylor, and W. Zhang, "Thin-film sensing with planar terahertz metamaterials: sensitivity and limitations," Opt. Express **16**(3), 1786–1795 (2008).
13. C. Rockstuhl, F. Lederer, C. Etrich, T. Zentgraf, J. Kuhl, and H. Giessen, "On the reinterpretation of resonances in split-ring-resonators at normal incidence," Opt. Express **14**(19), 8827–8836 (2006).
14. T. D. Corrigan, P. W. Kolb, A. B. Sushkov, H. D. Drew, D. C. Schmadel, and R. J. Phaneuf, "Optical plasmonic resonances in split-ring resonator structures: an improved LC model," Opt. Express **16**(24), 19850–19864 (2008).

#210799 - $15.00 USD Received 25 Apr 2014; revised 6 Jun 2014; accepted 6 Jun 2014; published 20 Oct 2014

15. S. Chiam, R. Singh, J. Gu, J. Han, W. Zhang, and A. Bettiol, "Increased frequency shifts in high aspect ratio terahertz split ring resonators," Appl. Phys. Lett. **94**(6), 064102 (2009).
16. S. Chiam, R. Singh, W. Zhang, and A. A. Bettiol, "Controlling metamaterial resonances via dielectric and aspect ratio effects," Appl. Phys. Lett. **97**(19), 191906 (2010).
17. F. Romanato, L. Businaro, L. Vaccari, S. Cabrini, P. Candeloro, M. De Vittorio, A. Passaseo, M. T. Todaro, R. Cingolani, E. Cattaruzza, M. Galli, C. Andreani, and E. Di Fabrizio, "Fabrication of 3D metallic photonic crystals by X-ray lithography," Microelectron. Eng. **68**, 479–486 (2003).
18. S. Gorelick, V. A. Guzenko, J. Vila-Comamala, and C. David, "Direct e-beam writing of dense and high aspect ratio nanostructures in thick layers of PMMA for electroplating," Nanotechnology **21**(29), 295303 (2010).
19. W. Withayachumnankul and D. Abbott, "Metamaterials in the terahertz regime," IEEE Photon. J. **1**(2), 99–118 (2009).
20. H. O. Moser, B. D. F. Casse, O. Wilhelmi, and B. T. Saw, "Terahertz response of a microfabricated rod-split-ring-resonator electromagnetic metamaterial," Phys. Rev. Lett. **94**(6), 063901 (2005).
21. B. D. F. Casse, H. O. Moser, J. W. Lee, M. Bahou, S. Inglis, and L. K. Jian, "Towards three-dimensional and multilayer rod-split-ring metamaterial structures by means of deep x-ray lithography," Appl. Phys. Lett. **90**(25), 254106 (2007).
22. C. Y. Chen, S. C. Wu, and T. J. Yen, "Experimental verification of standing-wave plasmonic resonances in split-ring resonators," Appl. Phys. Lett. **93**(3), 034110 (2008).
23. C. Enkrich, M. Wegener, S. Linden, S. Burger, L. Zschiedrich, F. Schmidt, J. F. Zhou, T. Koschny, and C. M. Soukoulis, "Magnetic metamaterials at telecommunication and visible frequencies," Phys. Rev. Lett. **95**(20), 203901 (2005).
24. N. Yu, P. Genevet, M. A. Kats, F. Aieta, J. P. Tetienne, F. Capasso, and Z. Gaburro, "Light propagation with phase discontinuities: generalized laws of reflection and refraction," Science **334**(6054), 333–337 (2011).
25. L. Rayleigh, "On the dynamical theory of gratings," Proc. R. Soc. A Math. Phys. Eng. Sci. **79**, 399–416 (1907).
26. B. Luk'yanchuk, N. I. Zheludev, S. A. Maier, N. J. Halas, P. Nordlander, H. Giessen, and C. T. Chong, "The Fano resonance in plasmonic nanostructures and metamaterials," Nat. Mater. **9**(9), 707–715 (2010).
27. X. F. Ang, F. Y. Li, W. L. Tan, Z. Chen, C. C. Wong, and J. Wei, "Self-assembled monolayer for reduced temperature direct metal thermocompression bonding," Appl. Phys. Lett. **91**(6), 061913 (2007).

1. Introduction

The Split Ring Resonator (SRR) is one of the first and most studied structures for metamaterials [1–5]. The SRR was originally designed to constitute the unitary cell of metamaterials showing a negative effective magnetic permeability in the microwave spectral range [6]. However, due to its morphology, the SRR is able to confine and enhance the electromagnetic field even outside this frequency range. In particular, when we consider the response of a nanometric SRR to an electromagnetic radiation, having a wavelength comparable to its size, the SRR shows interesting plasmonic resonances. Moreover, the large electric field enhancement, the variation of the response depending on the dielectric material surrounding the SRR, the possibility to excite multiple resonances, suggest the application of this geometry in the plasmonic sensing field [7–12].

Most of the work found in SRRs literature concerns relatively thin structures, usually few tens of nanometers thick [4,10,13]. Besides the very well-known fundamental LC resonance [14], it has been also pointed out several times that these SRRs present a number of further high-order resonances, which are found exploring the response at higher frequencies. In particular, for sub-micrometric SRRs, these resonances fall within the VIS-NIR part of the spectrum, and have been associated with a plasmonic behavior [13].

To our knowledge, only few analyses of the optical response of thick SRRs have been presented [9,15]. The spectral features that arise in this case were only partially explained, either by trying to extend the commonly employed LC model [16] or by means of qualitative reasoning [9]. Nonetheless, SRR thickness represents an interesting degree of freedom in the SRR geometry, which may allow to tune and to enrich the optical properties of these nanostructures.

In this work we perform a detailed analysis of the evolution of the SRR optical response with increasing of the SRR thickness, in a range of wavelength comparable to the structure's period (the visible and near-infrared range). The analysis, based on finite elements simulations, compares the scattering properties with a simple Fabry-Perot resonance model, which proves to catch the main new spectral features that arise for large SRR thicknesses.

#210799 - $15.00 USD Received 25 Apr 2014; revised 6 Jun 2014; accepted 6 Jun 2014; published 20 Oct 2014

Moreover, the interaction of these new resonances with the classical optical resonances of the SRR introduces interesting hybridizations, yielding sharper spectral features which may find potential sensing applications.

In order to finely control the geometry of the fabricated structure, we developed a X-ray Lithography based process [17]. This choice allowed us to produce high aspect ratio dense SRRs arrays on a transparent substrate, with very uniform geometrical characteristics over larger areas compared to other fabrication techniques, such as Electron Beam Lithography [18]. Moreover, this fabrication process inherently permits to produce high quality structures with sub-micrometric dimensions [19–21], which consequently allows a reliable characterization in the visible and near-infrared region. This is witnessed by the comparison of the obtained transmittance data with FEM simulations, which shows an excellent agreement.

We finally propose the result of a detection test, performed comparing the transmittance spectra before and after a biomolecule monolayer deposition. As expected from theory, we experimentally find the most sensitive configurations characterized by the simultaneous presence of horizontal and vertical SRR resonances, demonstrating the utility of thickness in improving the optical performances of SRR arrays.

2. Design and simulation

A scheme of the considered SRR array is reported in Fig. 1. Its optical response has been studied by means of the finite element method, using the software COMSOL Multiphysics. The simulated structure replicates the fabricated one: a gold split ring resonator over a bilayer of Indium Tin Oxide (100nm) and glass. Refractive indices of gold, ITO and glass, as well as the ITO thickness were previously measured by spectroscopic ellipsometry. The SRR lateral size is l = 390nm, width w = 120nm, gap size d = 60nm and period a = 460nm (Fig. 1, inset). We considered non-zero curvature radii for the vertical edges, in such a way to reliably reproduce the shape of the fabricated structures (see Fig. 7). Periodic boundary conditions were set at the unitary cell sides, while Perfectly Matched Layers were placed above and below to absorb scattered radiation. We solved the full three dimensional scattering problem in the case of normally impinging plane waves for two polarizations: perpendicular and parallel to the gap-bearing side, respectively denoted as x- and y-polarization from now on, according to the axes defined in Fig. 1.

The optical spectrum of such a SRR array is particularly rich (Fig. 2). This is mainly due to the coupling of impinging light to two classes of plasmonic resonances. We first address the first class by considering the case of thin SRR array: in this case, surface plasmon polaritons (SPP) modes are excited at the horizontal SRR surfaces, in particular the uppermost one (gold-air interface), which is directly illuminated. These optical resonances in SRR have been observed by several authors [4,13,22,23]. In these papers, thin (tens of nanometers thick) SRR were considered, illuminated by light in the VIS-IR spectral ranges. To understand the resonant mechanism, a simple resonant Fabry-Perot model has been proposed, which can be summarized with the well-known condition:

$$n_{SPP} k_0 L + \phi = \pi m \tag{1}$$

#210799 - $15.00 USD Received 25 Apr 2014; revised 6 Jun 2014; accepted 6 Jun 2014; published 20 Oct 2014

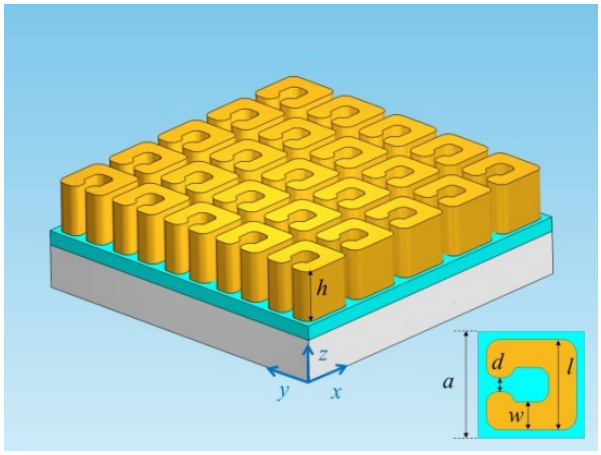

Fig. 1. Scheme of the gold SRR array on ITO covered glass; inset: top view of the unitary cell of the SRR array.

where k_0 is the vacuum wave vector, n_{SPP} is the effective mode index of the horizontal SPP modes propagating along the horizontal SRR surface, L is the optical path of the resonance, ϕ is the phase pick-up of the SPP at reflection at path terminations, and m is an integer. As pointed out by Rockstuhl et al. [13], odd-m resonances are excitable for impinging light polarization parallel to the gap-bearing side of the SRR, while even-m resonances arise in case of orthogonal polarization. As it was pointed out [4,13], moreover, different resonant paths are possible. One path is the average length of the "C" shape of the SRR ($L = 4(l\text{-}w)\text{-}g$), another one corresponds to the SRR sides without gap, and still another one to the small arms of SRR along the gap bearing side of the SRR. The superposition of all of these resonances produces the complicated systems of peaks and dips found for small thicknesses [13].

In order to highlight the different horizontal resonant paths, we simulated the response of an array of thin SRRs. Figures 2(a) and 2(b) refer to the case of SRR of thickness 40nm illuminated respectively by x- and y-polarized light. We report the spectra of the reflectance, the absorptance and the maximum of field enhancement in the air domain around the structure (max(|**E**|)), as a function of the impinging light wavelength. The enhancement is calculated with respect to the impinging light field. The peaks found in the spectra of absorptance and max(|**E**|), in particular, can be directly correlated to a resonance excitation, while reflectance peaks location additionally depends on the phase of the resonantly scattered wave [24].

In case of x-polarization (Fig. 2(a)), the main peak of max($|\mathbf{E}|$) is related to the $m = 3$ resonance relative to the x-oriented sides of the SRR, as it is clear from the $|\mathbf{E}|$ field distribution (Fig. 2(a), inset). On the other hand, in the case of y-polarization, Fig. 2(b), a large number of resonances are found. They are respectively the resonance $m = 3$ of the y-oriented SRR side (inset 1), resonances $m = 5$ and $m = 3$ of the whole "C" shaped pattern (insets 2 and 5), and resonances of the small arms of the in the gap-bearing side of the SRR (insets 3 and 4).

In our case, the optical response is made more complex by the relatively large width of our SRR structure ($w = 120$nm, twice the one considered for example in [13]), which tends to merge and smooth the spectral features, and by the small distance between adjacent SRRs, which determines near field coupling between SRRs.

With increasing SRR thickness several new spectral features arise. Reflectance and absorptance maps as a function of SRR thickness and impinging light wavelength are reported in Figs. 2(c)–2(f). For what concerns the first class of resonances, however, we notice that an important role is played by the $m = 3$ resonance of the "C" structure (Fig. 2(b), inset 5).

#210799 - $15.00 USD Received 25 Apr 2014; revised 6 Jun 2014; accepted 6 Jun 2014; published 20 Oct 2014

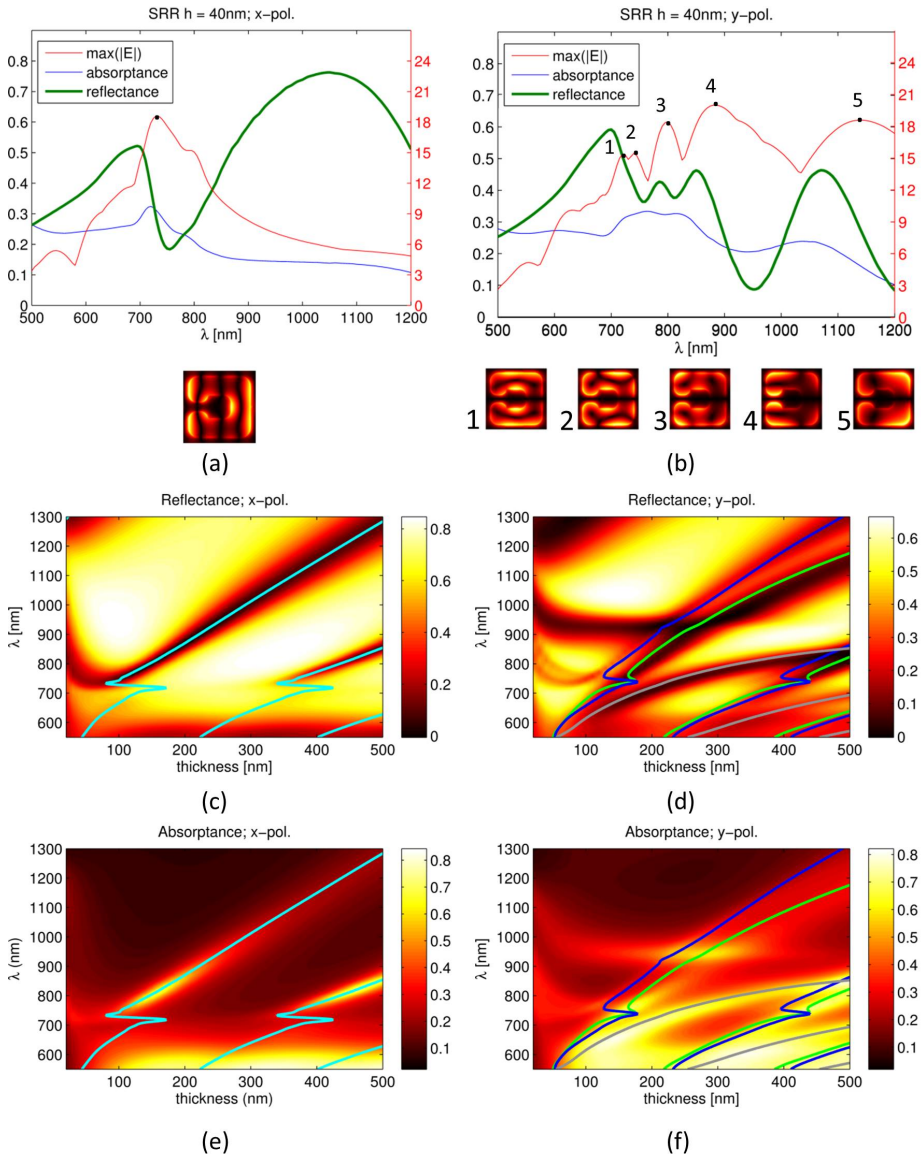

Fig. 2. (a) Reflectance (green), absorptance (purple) and maximum field enhancement, max(|E|), (pink) spectra as a function of wavelength, in the case of SRR thickness of 40nm, for x- (left) and y-polarization (right). Insets: |E| field maps. Reflectance (left, (a) and (c)) and absorptance (right, (b) and (d)) maps as a function of SRR thickness and wavelength for normally impinging light, polarized orthogonal (above, (a) and (b)) and parallel (below, (c) and (d)) to the gap bearing side. Superimposed lines mark the Fabry-Perot resonances of the corresponding modes, reported in Fig. 4.

In fact, looking in particular at the absorptance map (Fig. 2(f)), it can be seen that, unlike the other ones, this resonance takes place even at higher SRR thicknesses. While for thin SRR this resonance is located at $\lambda = 1150$nm, with the increasing of the geometry height its spectral location stabilizes at $\lambda = 950$nm, almost independently of the SRR thickness.

What clearly stands out from the maps is the presence of a set of resonances which strongly depends on the SRR thickness. The nature of these resonances is, however, similar to the previous one. As a matter of fact, in this case 'vertical' Fabry-Perot resonances are

#210799 - $15.00 USD Received 25 Apr 2014; revised 6 Jun 2014; accepted 6 Jun 2014; published 20 Oct 2014

involved, due to SPP modes of the SRR array bouncing back and forth between the two horizontal metal dielectric interfaces.

In order to support this interpretation, we performed a numerical modal analysis of the SRR cross section, i.e. we looked at the possible optical modes propagating along the z axis (see Fig. 1) assuming infinitely long SRRs.

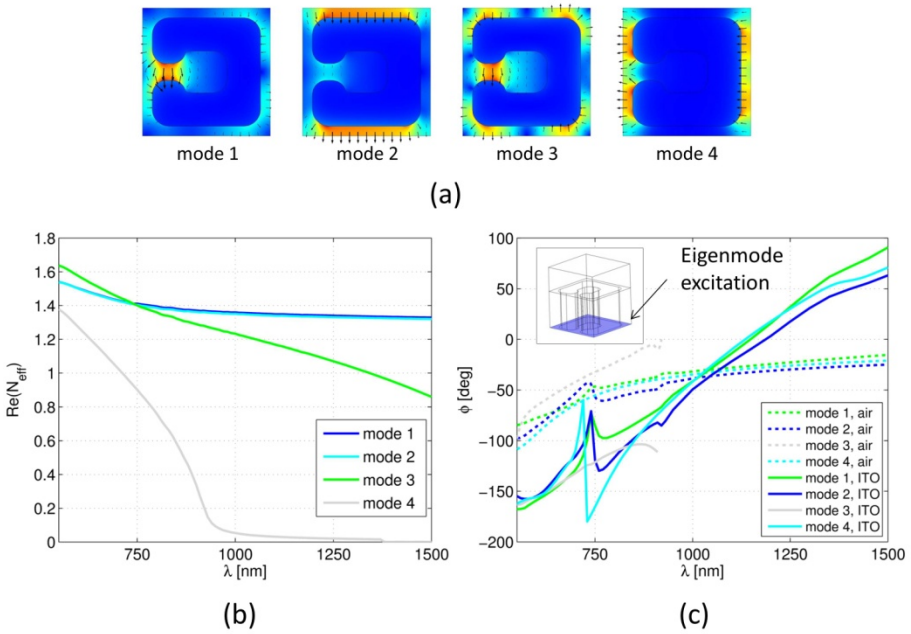

Fig. 3. (a) Eingenmodes field norm profiles at λ = 800nm. (b) Effective index (N_{eff}) of SRR optical modes propagating along the z axis. (c) Reflection phases of the modes.

Four modes have been found analyzing the cross section of the SRR (Fig. 3(a)). These eigenmodes are found in the form $\mathbf{E}_i(x,y,z) = \mathbf{E}_i(x,y)\exp(ik_0 N_i z)$, being N_i the effective mode index of the *i*-th mode. The dispersion of the modes as a function of wavelength is reported in Fig. 3(b), together with the eigenmodes fields at the sample wavelength of 800nm (Fig. 3(a)).

As it can be seen from Fig. 3(a), a single mode, the 4th, is expected to be compatible with impinging light polarized orthogonal to the gap-bearing side (x-polarization), whose field is mainly concentrated between a SRR and the adjacent ones. Therefore, the gap is expected to play no role in the optical response for this polarization. On the other hand, light polarized parallel to the gap-bearing side (y-polarization) may couple to three main modes, two of them, the 1st and 3rd, showing a high field concentration within the gap.

Once impinging light couples to these modes, they undergo a Fabry-Perot resonant mechanism, bouncing back and forth between the SRR horizontal boundaries,

$$2hk_0 N_i + \phi_i^{air} + \phi_i^{ITO} = 2m\pi \qquad (2)$$

where *h* is the SRR thickness, ϕ^{air} and ϕ^{ITO} are the reflection phases of the modes at the respective SRR termination and *m* is an integer.

In order to directly compare this interpretative model with scattering simulations, the phases ϕ^{air} and ϕ^{ITO} for each mode need to be explicitly calculated as a function of wavelength. Then, Eq. (2) can be numerically solved for each mode and integer *m*, being the SRR thickness *h* the only unknown. The calculation was performed by considering the 3D FEM model depicted in Fig. 3(c) (inset), which explicitly simulates the reflection of the *i*-th

#210799 - $15.00 USD Received 25 Apr 2014; revised 6 Jun 2014; accepted 6 Jun 2014; published 20 Oct 2014

mode at single SRR array terminations. The *i*-th eigenmode is launched by means of a port boundary excitation at the SRR base. The mode, then, propagates toward the SRR ending and gets reflected back to the port. The scattering parameter S_{ii} is calculated by the software as:

$$S_{ii} = \frac{\int_{port} (\mathbf{E}_{tot,i} - \mathbf{E}_i) \cdot \mathbf{E}_i^* ds}{\int_{port} \mathbf{E}_i \cdot \mathbf{E}_i^* ds} = \frac{\int_{port} \mathbf{E}_i R_i \exp(i2Hk_0 N_i) \cdot \mathbf{E}_i^* ds}{\int_{port} \mathbf{E}_i \cdot \mathbf{E}_i^* ds}$$
$$= \frac{R_i \exp(i2Hk_0 N_i) \int_{port} \mathbf{E}_i \cdot \mathbf{E}_i^* ds}{\int_{port} \mathbf{E}_i \cdot \mathbf{E}_i^* ds} = R_i \times \exp(i2Hk_0 N_i) \quad (3)$$

where ($\mathbf{E}_{tot}$-$\mathbf{E}_i$) is the difference between the full calculated electric field at the port and the *i*-th eigenmodes field, *H* is the portion of SRR thickness considered in the simulation and R_i is the complex reflection coefficient of the mode at the SRR termination. The latter can be written as

$$R_i = \rho_i \exp(i\phi_i) \quad (4)$$

The reflection phase ϕ_i is then obtained from S_{ii} as:

$$\phi_i = \arg\left[S_{ii} \exp(-2iHk_0 N_i)\right] \quad (5)$$

We carried out the calculation in both the cases of presence of air and ITO as dielectric media at the SRR terminations, in order to obtain ϕ^{air} and ϕ^{ITO}, which are reported in Fig. 3(c).

We notice that the second and the fourth modes show a reflection phase discontinuity at λ~725nm, which is related to the Wood's anomaly [25] for the first diffraction order for a grating with pitch 460nm in ITO environment (ref. index ~1.565).

In Figs. 2(c)–2(f) the solid lines superimposed to the maps mark the solutions of Eq. (2), considering the numerically calculated effective mode indices and reflection phases. A good agreement is found between the model and scattering simulation. Most of the reflectance dips at high SRR thicknesses are reproduced by the model, which confirms the preponderant Fabry-Perot resonant mechanism in determining the optical response of the SRR array.

Finally, we want to investigate the potentialities of the considered thick SRR array as a sensing structure. In order to quantify the sensitivity of the SRR array to a change in refractive index of the surrounding environment, we consider as a figure of merit the transmittance variation $\Delta T = |T_{1.000} - T_{1.001}|$, where $T_{1.000}$ and $T_{1.001}$ are the transmittances with environment dielectric constants set to n = 1.000 and 1.001 respectively.

Figure 4 reports the Transmittance (T) and ΔT maps for x- and y-polarized light. As it can be seen from the color scale, light polarized orthogonal to the gap yields a much higher maximum sensitivity to refractive index variations than the x-polarization case. Comparing these maps with the reflectance maps (Fig. 2(c), 2(d)), it is clear that the highest sensitivity regions are found along the Fabry-Perot resonances of the structure. An additional high sensitivity region is found along the aforementioned SRR localized resonance (λ ~950nm). Interestingly, the maximum sensitivitiy in the considered parameters ranges is found at the crossing point between the SRR localized resonance and the Fabry-Perot resonances (*h* = 250nm, λ = 930nm), similarly to what has been reported for other plasmonic grating structures presenting multiple resonant patterns [26].

#210799 - $15.00 USD Received 25 Apr 2014; revised 6 Jun 2014; accepted 6 Jun 2014; published 20 Oct 2014

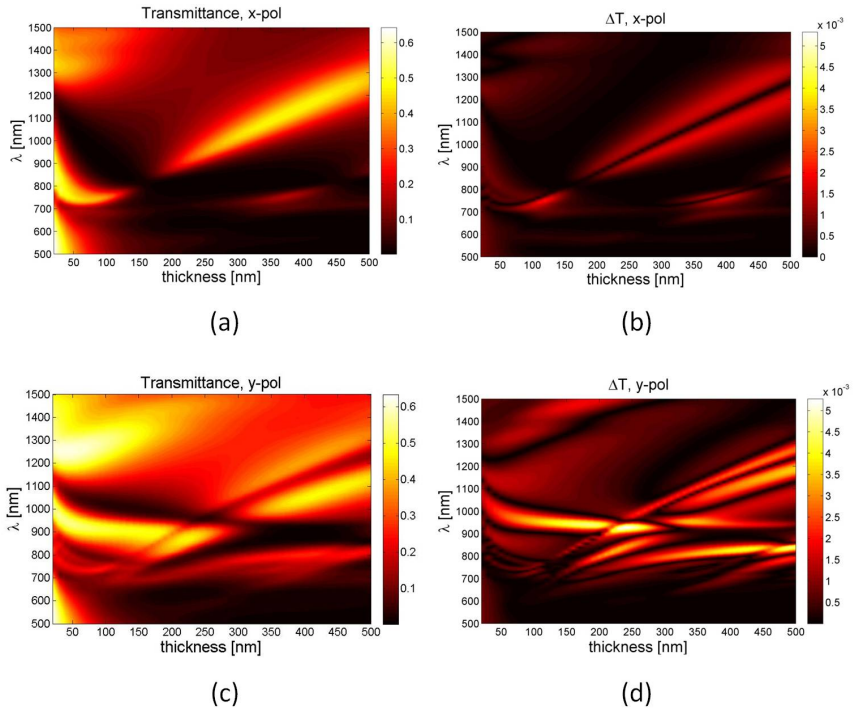

Fig. 4. SRR array transmittance (left, (a) and (c)) and transmittance variation $\Delta T = |T_{1.000} - T_{1.001}|$ (right, (b) and (d)) as a function of the thickness and wavelength, for x-polarized (above, (a) and (b)) and y-polarized (below, (c) and (d)) impinging light.

3. Fabrication

The goal of the fabrication was the production of a set of large dense arrays of gold nano-metric SRRs on transparent substrate, the only parameter changing between the chips being the gold thickness. We exploited the X-ray lithography (XRL) as the main fabrication technique, since it allows to obtain large (up to few centimeters square) lithographed areas in a single exposure and to impress relatively thick photoresist layer (up to tens of micrometers), maintaining a high resolution. The X-ray mask was produced by Electron Beam Lithography (EBL) on silicon nitride membrane and electrochemical growth. The pattern produced on the mask was replicated on a transparent substrate by means of XRL and electrochemical growth of gold.

The use of polymethylmethacrylate (PMMA) as photoresist, both for EBL and XRL, was due to the high resolution required for the lithographic processes. EBL process for producing the X-ray mask was performed on PMMA (Allresist AR671.05) covered silicon nitride membrane, using a JEOL EB6300FS EBL in HR. The area of the SRR array chip is 1 × 1mm. XRL was performed on PMMA on ITO covered glass, in soft x-ray regime (1-2keV). This bi-layer was chosen as sample substrate in order to achieve transmission measurements, since it is transparent in the range of interest (400-1100 nm wavelength). In order to enhance PMMA adhesion on ITO, we spun a thin (<20nm) layer of diluted SAL (Microposit SAL607) on the substrate before PMMA deposition. After the exposure and the development of

#210799 - $15.00 USD Received 25 Apr 2014; revised 6 Jun 2014; accepted 6 Jun 2014; published 20 Oct 2014

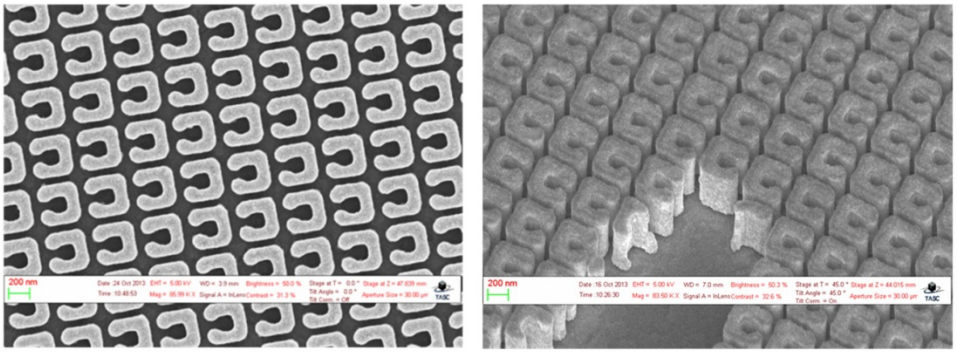

Fig. 5. Top (a) and tilted (b) views SEM micrographs of positive tone gold SRRs on ITO covered glass, fabricated by XRL and electrochemical gold growth. SRR features: period a = 460nm, side l = 390nm, width w = 120nm, gap d = 60nm, height h = 360nm. The height of the structure was measured on a defect of the array (b), normally present due to the lithographic process and not affecting the optical measurements.

PMMA, the layer of SAL was removed by a reactive ion etching process based on O_2/CF_4 gas mixture.

Finally, the gold was deposited by electrochemical growth and the resist template removed. Scanning Electron microscopy images of a detail of the SRRs array are reported in Fig. 5.

4. Characterization and detection test

The validity of the simulated results were checked by measuring the response of the fabricated SRRs array through transmittance measurements, performed by means of a VASE (J.A. Woollam) Spectroscopic Ellipsometer. The transmittance spectra have been collected at normal incidence for x- and y-polarization.

The comparison of the simulated and experimental (Fig. 6) spectra shows an excellent qualitative agreement. The slight mismatch may be due to the discrepancies between the simulated model and the real sample: inaccuracies in the fabricated SRR, inhomogeneities in the SRRs array, deviation of the refractive index values used in the simulation from the real ones and imprecise linear polarization tuning along the x and y axis of the SRR arrays.

Despite these numerous sources of error, we noticed that almost all of the predicted spectral features, due to multiple Fabry-Perot resonances, are actually experimentally found with very similar absolute and relative intensities. The agreement is better for x-polarization than for the y- one. This can be understood since in y-polarization two of the three excitable modes have high electric fields inside the gap (see Fig. 3(a)) and are therefore expected to be sensitive to the gap width, which is slightly different between the different samples. On the other hand, for the sake of simplicity, the simulations assumed a fixed average gap geometry.

To experimentally investigate the sensing potential of the structure, we performed a detection test using a biomolecule monolayer. A self-assembled monolayer of dodecanethiol ($C_{12}H_{25}SH$) was deposited on the SRRs' surface at room temperature. The substrate was pre-cleaned in a basic peroxide solution (5:1:1 double distilled H_2O, 30% H_2O_2 and 25% NH_4OH) for 5 minutes, rinsed in double distilled water and dried under N_2 flux. The cleaned sample was submerged in 6 mM solution of dodecanethiol in ethanol for about 48 hrs and therefore rinsed thoroughly with ethanol for at least 4 minute, followed by drying under nitrogen stream. The spontaneous assembly of the molecules is known to form a densely packed and highly oriented structure on a metallic surface [27].

#210799 - $15.00 USD Received 25 Apr 2014; revised 6 Jun 2014; accepted 6 Jun 2014; published 20 Oct 2014

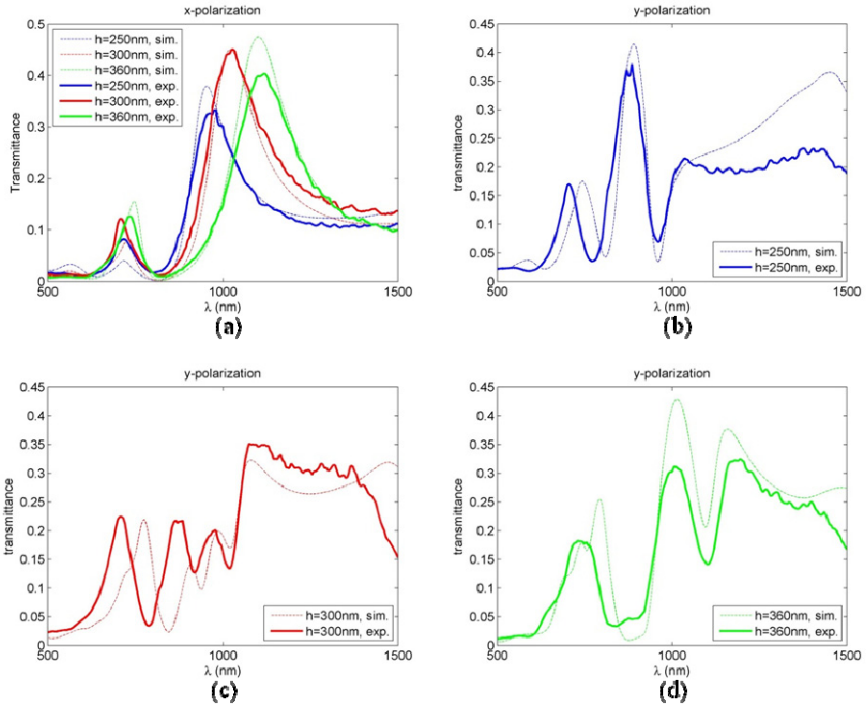

Fig. 6. Transmittance spectra for SRR with thickness 250 (blue), 300 (red) and 350nm (green) for x-polarized (a) and y-polarized (b, c, d) light. Thick and thin solid lines mark respectively experimental and simulated spectra.

In Fig. 7 we report transmittance spectra corresponding to SRR thicknesses of 250nm, 280nm, 300nm and 360nm before and after functionalization for x- and y-polarized light. After the functionalization, a 10nm red-shift was observed for the main transmittance peak in x-polarization, while an average of 20nm red-shift was observed for the central transmittance peak in y-polarization. The highest transmittance variations were expected in case of y-polarization and for the SRR thickness close to the optimal one, as predicted by simulation, namely h = 250nm. In this configuration, the interference between horizontal and vertical resonances of the SRR structure determines a set of three peaks in transmittance, the central one having the highest slopes.

The expected scenario was actually found experimentally. The transmittance variation $|\Delta T| = T_{bare} - T_{funct}$, reported below the spectra, clearly shows higher values for the y-polarization than for x-polarization. Moreover, referring to the central transmittance peak, the highest transmittance variations are actually found for h = 250nm and 280nm, i. e. close to the predicted one. By contrast, we notice that the non-optimal samples with h = 300nm and h = 360nm show much lower shifts and $|\Delta T|$ values, as expected.

Although this is just a test, it demonstrates that the possibility to combine the well-known SRR horizontal optical resonances with vertical Fabry Perot resonances in thick SRR opens up new possibilities for increase the sensitivity of these structures as sensing plaforms.

#210799 - $15.00 USD Received 25 Apr 2014; revised 6 Jun 2014; accepted 6 Jun 2014; published 20 Oct 2014

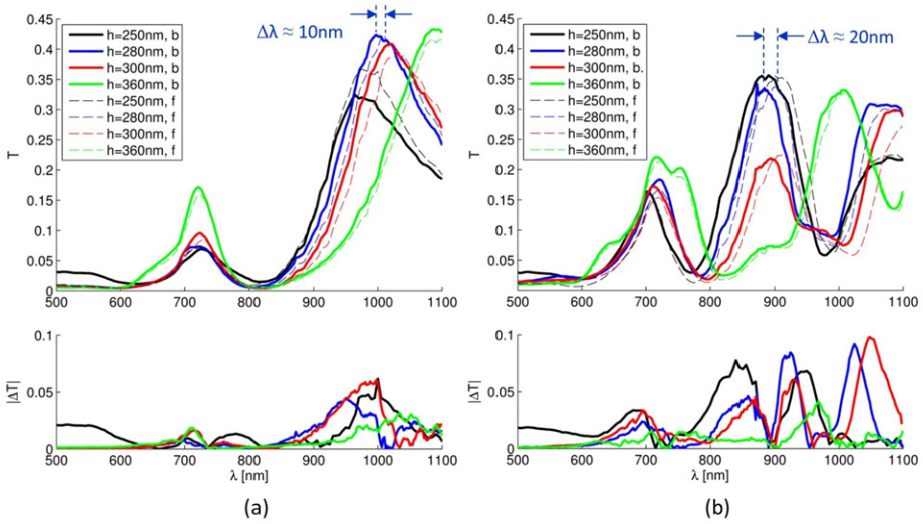

Fig. **7**. Above: Transmittance spectra for SRR with thickness 250 (black), 280 (blue), 300 (red) and 360nm (green) for x-polarized (a) and y-polarized (b) light. Solid and dotted lines mark respectively before and after functionalization spectra. Below: Transmittance variation for SRR with thickness 250 (black), 280 (blue), 300 (red) and 360nm (green) for x-polarized (a) and y-polarized (b) light.

5. Conclusions

In this work we investigated the plasmonic response of thick dense SRR arrays in the visible and near-infrared range (400-1100nm). We analyzed the case of normally impinging plane wave with electric field polarized parallel and perpendicular to the gap-bearing side, focusing our attention on an accurate explanation of the resonant mechanism of the SRR geometry. We pointed out the presence of two different classes of plasmonic resonances, one produced by the SPP modes excited at the horizontal surface of the SRR, another due to "vertical" Fabry-Perot resonances, caused by the SPP modes bouncing back and forth between horizontal metal dielectric interfaces. Our analysis explains in detail the spectral features arising in the case of thick SRRs, which have only been explained partially in previous studies.

The fabrication process was optimized in order to obtain in a fast process large area samples with good lithographic quality at the nanoscale.

Since the SRR thickness represents an interesting degree of freedom in the SRR geometry, the potentialities of the tall SRRs array as a sensing structure were analyzed both theoretically and experimentally, identifying in both cases the maximum sensitivities at the crossing point between the localized resonance and the Fabry-Perot resonances. The comparison of the simulated and experimental spectra shows an excellent qualitative agreement.

Acknowledgments

This work has been supported by SPLENDID project (Surface PLasmonics for Enhanced Nano-Detectors and Innovative Devices) by CARIPARO foundation.

#210799 - $15.00 USD Received 25 Apr 2014; revised 6 Jun 2014; accepted 6 Jun 2014; published 20 Oct 2014